IEEE Photonics Journal
An IEEE Photonics Society Publication

Open Access

Broadband Polarization-Insensitive Metamaterial Perfect Absorbers Using Topology Optimization

Volume 8, Number 5, October 2016

Sze Ming Fu
Yan Kai Zhong
Nyan Ping Ju
Ming-Hsiang Tu
Bo-Ruei Chen
Albert Lin

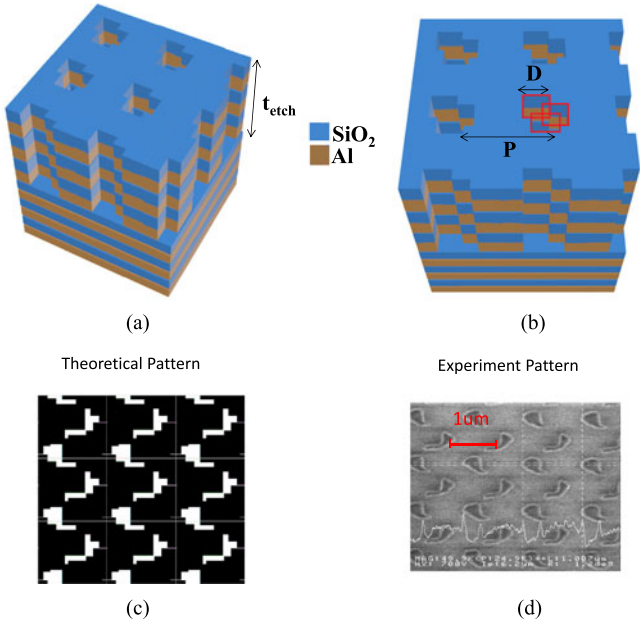

DOI: 10.1109/JPHOT.2016.2602335
1943-0655 © 2016 IEEE

IEEE photonics SOCIETY

IEEE

Broadband Polarization-Insensitive Metamaterial Perfect Absorbers Using Topology Optimization

Sze Ming Fu, Yan Kai Zhong, Nyan Ping Ju, Ming-Hsiang Tu, Bo-Ruei Chen, and Albert Lin

Department of Electronic Engineering, National Chiao-Tung Univeristy, Hsinchu 30010 Taiwan

DOI:10.1109/JPHOT.2016.2602335

Manuscript received July 16, 2016; revised August 14, 2016; accepted August 18, 2016. Date of publication August 24, 2016; date of current version September 8, 2016. The work was supported by the Ministry of Science and Technology (MOST), Taiwan, under Grant MOST-104-2221-E-009 -115 -MY2. Corresponding author: A. Lin (e-mail: hdtd5746@gmail.com).

Abstract: A novel scheme for a perfect hyperbolic metamaterial (HMM) absorber is proposed, and experimental verification is provided. It has been shown previously that tapered HMM stacks can provide adiabatic waveguiding over a wide spectral range and thus are an ideal opaque absorber. Here, nontapered shape-optimized HMM absorbers are proposed, which facilitates the fabrication and promotes the large-area applications such as thermophotovoltaics (TPV). In the synthesis of the optimal patterns, we use 5-harmonic rigorously coupled wave analysis (RCWA) and experimental trials to shorten the trial-and-error time. The best pattern provides an averaged broadband experimental absorption of 88.38% over $\lambda = 1$ μm to $\lambda = 2$ μm, which is comparable to the state-of-the-art experimental effort using tapered HMM. The nontapered nature can be easier to fabricate from the semiconductor processing viewpoint. The physics behind the pattern-optimized HMM cavity is the broadband light coupling by the air-cavity and the unbounded photonic density of the states (PDOS) associated with the HMM. The topology optimized air cavity effectively couples the incident photons into the metal-dielectric stacking, eliminating the need of sidewall tapers. We believe the proposed topology-optimization methodology benefits the future design of compact metamaterial perfect absorbers (MPA), sensors, antenna, and thermophotovoltaic emitters, and absorbers.

Index Terms: Diffractive optics, metamaterials, photovoltaic, plasmonics, silicon nanophotonics.

1. Introduction

Metamaterial perfect absorbers (MPAs) have been an important research subject due to the potential applications in highly sensitive sensors, ultrafast modulators, antenna systems, thermal emitters [1], and thermophotovoltaics [2] (TPV). The realization of a broadband MPA has been under extensive study at infrared [3], visible [4], [5], Tera-Hertz [6], and microwave frequencies. Hyperbolic metamaterial (HMM) is an artificial material with metal-like permittivity in one direction and dielectric-like permittivity in another direction [7]–[10]. Its hyperbolic band structure can lead to very high absorption over a broad wavelength range. Recently, Fang *et al.* proposed the use of a tapered HMM to implement perfect absorbers [11], where the calculated absorbance can be higher than 0.99 over the broad spectral range [10], [11]. The difficulty in the implementation of semicon-

ductor tapered structure is the fabrication issues. At each layer, lithography and etching are needed in order to realize tapered structures. Theoretical result using $N = 20$ alternating layers reports high broadband absorption [11]. Nonetheless, fabricating $N = 20$ tapered structures for large-area applications is quite difficult, especially if the taper angle has to be precisely controlled for wavelength scalability. The experimentally realized MPA using tapered HMM can achieve around 90% absorbance [9], [10]. In this work, the tapered HMM structure is replaced by a new type of cavity-type MPA with topology optimization, and the experimental absorbance achieved is comparable to the fabricated tapered HMM MPAs [9], [10]. The theoretical and experimental results are provided and its decent feasibility and scalability to large devices are reflected in its simple and ordinary lithography and etching processes. The non-tapered nature makes its scalable for large-area TPV applications and fits to common low-cost lithography techniques including nano-imprint (NIL) and photo-lithography, in addition to e-beam lithography.

The topology optimization has been proved to be effective in nano-photonic problems [12]–[18]. In the past, random-texture based optimization has been studied based on various optimization algorithm [13], [14]. The advantage of the random-texture based photonic design is its similarity to a Lambertian surface where random light scattering and the corresponding cosine emission can be very effective for nano-photonic absorption enhancement. The slight drawback is the fabrication difficulty in reproducing the designed texturing in experiments. On the other hand, aperiodic designs using gratings of different periods are shown to be more effective than periodic patterns [15], [16]. In the aperiodic grating design, step-like gratings are mostly used, and the design flexibility is in the grating period while the etching depth is uniform. This prevents the difficulty in fabrication. A more evolved scheme over aperiodic design is the topology design using bitwise step-like one-dimensional or two-dimensional patterning [12], [17], [18]. The bitwise step-like patterning is an alternative way to the random surface texture to achieve absorption enhancement. From the viewpoint of photonic design, the random surface texturing is the most effective due to its largest design degree of freedom and the most similarity to a true Lambertian surface. Nevertheless, the bitwise step-like design alleviates the fabrication difficulty. In this proposal, we propose a topology optimization for broadband MPAs for the first time. The bitwise binary grid is not used, and the superposition of geometrical elements is employed instead. The advantage over the bitwise pattern is the prevention of the isolated fine features that can always happen in the bitwise based optimization.

Fig. 1 illustrates the proposed design using topology-optimized HMM structures. Air holes are formed on the HMM stacks, and the resulting air-hole patterns are arranged in a two-dimensional array. The physics behind the perfect absorption over broadband wavelength range is somehow different from the tapered HMM stacks [11]. The non-tapered photonics nanostructure here eliminates the possibility of adiabatic coupling of the photons into the HMM stacks. Nonetheless, the shape-optimized air-cavity design enables the photon in-coupling and the photon trapping inside the HMM nano-structure. Since the HMM stack is still employed in this work, the photonic density of the state (PDOS) is still unbounded, which can also boost the broadband absorption. This leads to a broadband cavity-resonant HMM MPAs. While the resonant behavior is most of the time narrowband in nature, the hyperbolic dispersion facilitates the realization of broadband resonances. The surprising nature of the hyperbolic dispersion leads to a resonance that is reasonably strong and broadband at the same time. This somehow contradicts the conventional resonance behavior where high-Q modes tend to be narrowband and low-Q modes are of weak oscillation strength. Alternating aluminum (Al) and silicon dioxide (SiO_2) is used here with $N = 16$ pairs. In addition to the PDOS, another important factor to increase the broadband absorption is using complex photonic pattern design to enhance photon in-coupling. The pattern design is achieved by adjusting the side-length (D) and the position of $N_S = 10$ squares, using global optimization. The superposition of the squares forms a complex photonic pattern. Since random polarization exists for solar irradiance, the design of a polarization-insensitive-MPA is demonstrated here. The genetic algorithm (GA) is employed to globally optimize the parameters. The optimized geometry is $t_{Al} = 26.8$ nm, $t_{SiO2} = 18.2$ nm, and $t_{etch} = 360$ nm (8 pairs). The period (P), square side length (D), and the position of each square are included in Table 1. The number of squares (N_S) can be increased to enlarge

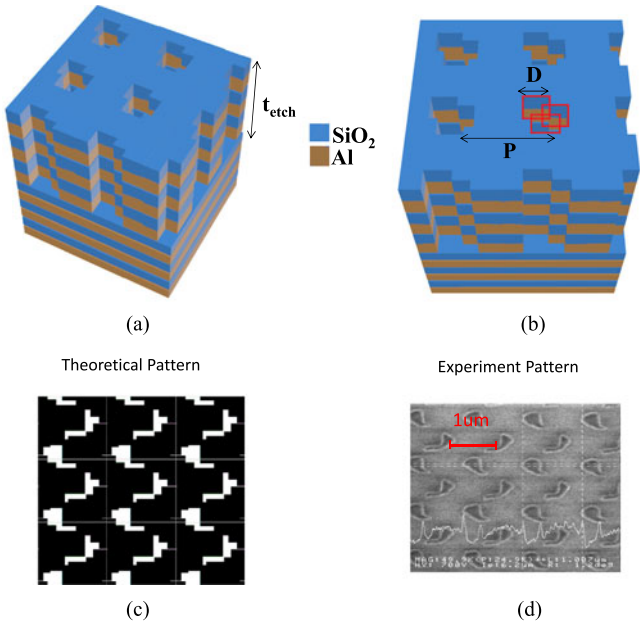

Fig. 1. (a) and (b) Non-tapered hyperbolic metamaterial (HMM) stacks for a metamaterial perfect absorber (MPA). The complex photonic pattern design is necessary to boost the absorbance. We use 5-harmonics 3-D RCWA calculation to shorten the experimental trial-and-error time. The combination of the simulation and experiment optimization is the most time-efficient. In the simulated and fabricated devices, $N_S = 10$ squares are used in this study. The metal used in this study is aluminum (Al). Noble metals such as silver or gold are not necessary. In addition, silver or gold is not compatible to silicon photonics process. D is the side length of an individual square, P is the period of the air-hole array, and t_{etch} is the etching depth. (c) Optimized topology in simulation and (d) the scanning electron microscopy (SEM) image of the fabricated pattern.

the searching space, but this requires more GA run time. The selection of the total deposited pair number $N = 16$ is based on the minimal pair number required for full absorption [9], [10]. For etching depth (t_{etch}), insufficient t_{etch} leads to imperfect photon confinement while excessive etching depth leads to process difficulty.

The averaged broadband absorbance is 88.38%, comparable to the state-of-the-art experimental effort using a tapered HMM stack [9], [10]. The easy-to-fabricate nature is the advantage of our design. Only one lithography and etching is needed to form the air-cavity HMM stack.

2. Methodology and Problem Set-up

The absorbance (A) for a specific polarization angle (Ψ_p) is calculated by integrating the power dissipation over the entire photonic device:

$$A_{\Psi_P}(\lambda) = \frac{\frac{1}{2}\int_V \omega\varepsilon_0\varepsilon''(\lambda)\left|\vec{E}_{\Psi_P}(\vec{r})\right|^2 dv}{\frac{1}{2}\int_S \mathrm{Re}\left\{\vec{E}_{\Psi_P}(\vec{r}) \times \vec{E}_{\Psi_P}^{\ *}(\vec{r})\right\} \cdot d\vec{s}} \tag{1}$$

where ω is the angular frequency, λ is the free space wavelength, ε_0 is the permittivity in vacuum, and ε'' is the imaginary part of the complex semiconductor dielectric constant. $E_{\Psi p}$ and $H_{\Psi p}$ is the electric and magnetic field intensity for a specific polarization of the incidence field. The material parameters are from Rsoft™ material database [19]. The calculation method is based on the rigorously coupled wave analysis (RCWA) implemented by Rsoft Diffractmode™. In many cases, the broadband response has to exist for randomly polarized light. For example, the solar irradiance possesses photons with all polarization angles. Therefore, in this study, we calculate an averaged absorbance value over all polarizations. The broadband absorption for the polarization averaged light incidence

TABLE 1

Square Center Positions (X, Y), and the Pattern Period (P) for the Topology Optimized MPAs. Unified square side length (D) is used in this study. $N_s = 10$ square is used in the GA optimization to form the complex photonic pattern. The unit is the micrometer (μm).

	X1	X2	X3	X4	X5	X6
1st GA run	0.2717	–0.4291	–0.3189	0.0354	–0.2874	–0.0118
2nd GA run	0.2323	–0.4291	–0.3031	0.0354	–0.0906	–0.0118
3rd GA run	0.3031	–0.4213	–0.3583	0.0118	–0.0906	–0.0197
	X7	X8	X9	X10	Y1	Y2
1st GA run	0.3819	0.0669	0.4370	–0.4764	0.4764	0.2717
2nd GA run	0.3819	0.1220	0.4449	0.4843	0.4764	0.2638
3rd GA run	0.3819	0.0591	0.4370	–0.2323	0.4843	0.2717
	Y3	Y4	Y5	Y6	Y7	Y8
1st GA run	–0.0748	–0.3740	0.2008	0.1378	–0.2480	–0.3110
2nd GA run	–0.0906	–0.3740	0.1772	0.1378	–0.2480	–0.3189
3rd GA run	–0.0354	–0.3740	0.2402	0.1220	–0.2402	–0.3425
	Y9	Y10	P	D	–	–
1st GA run	0.3661	–0.1220	0.9919	0.3757	–	–
2nd GA run	0.3661	–0.1220	0.9975	0.3762	–	–
3rd GA run	0.3661	–0.1299	1.0751	0.4089	–	–

is imperative for many applications such as geographical sensing, thermophotovoltaics (TPV), etc. Based on electromagnetic theory, the incidence electric field for 45°-polarized, circularly-polarized, and arbitrary polarization angle ($\vec{E}_{45,lin}$, $\vec{E}_{cir}$, $\vec{E}_{\Psi_P}$), can be expressed in terms of the s- and p-polarized incidence field ($\vec{E}_S$, $\vec{E}_P$)

$$\begin{aligned} \vec{E}_{45,lin} &= \frac{1}{\sqrt{2}}\vec{E}_s + \frac{1}{\sqrt{2}}\vec{E}_P \\ \vec{E}_{cir} &= \frac{1}{\sqrt{2}}\vec{E}_s + \frac{1}{\sqrt{2}}i\vec{E}_P \\ \vec{E}_{\Psi_p} &= a\vec{E}_s + b\vec{E}_P. \end{aligned} \tag{2}$$

In addition, the spectral absorbance (A_{Ψ_p}) can be calculated by knowing the spectral absorbance for s-, p-, 45°-polarized, and circularly-polarized spectral absorbance (A_s, A_p, A_{45}, A_{cir}) and using the following formula [20]:

$$\begin{aligned} A_{\Psi_P}(\lambda) = \frac{1}{a^2+b^2} \times [&a^2 A_s(\lambda) + b^2 A_p(\lambda) \\ &+ real(a^* b) \times (2A_{45,lin}(\lambda) - A_s(\lambda) - A_s(\lambda)) \\ &- imag(a^* b) \times (2A_{cir}(\lambda) - A_s(\lambda) - A_s(\lambda))] \end{aligned} \tag{3}$$

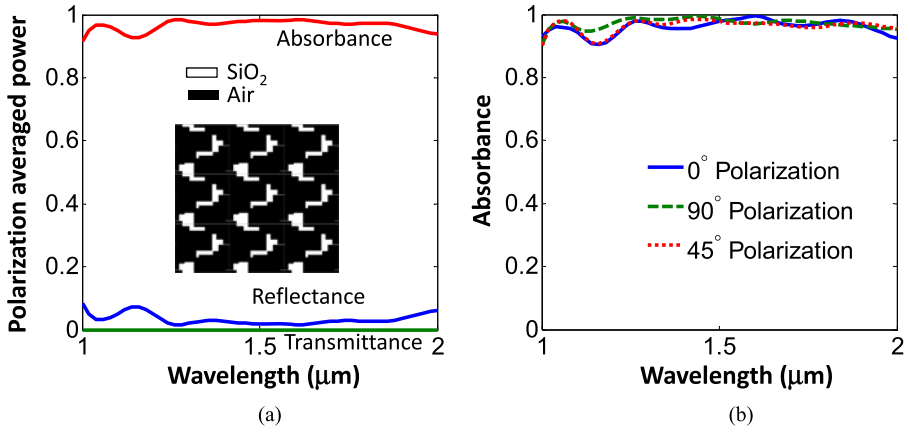

Fig. 2. Calculated broadband absorption of pattern-designed HMM MPA proposed in this study. (a) Polarization averaged spectral absorbance, reflectance, and transmittance. (b) Spectral absorbance for different polarizations. The target wavelength range is from $\lambda = 1$ μm to $\lambda = 2$ μm. The optimization is accomplished by a genetic algorithm (GA). The 5 harmonics is used in this RCWA simulation in both of the x- and y-direction since this is a 3-D RCWA simulation. (Inset) Optimized pattern after GA run. $t_{Al} = 26.8$ nm, $t_{SiO2} = 18.2$ nm, and $t_{etch} = 360$ nm (eight pairs). The other geometry is listed in the GA 3rd run row of Table 1. The polarization-averaged power is calculated using (3).

where *a* and *b* are the same quantities in (2). Equation (3) can also be used to calculate polarization-averaged spectral transmittance or reflectance. The polarization-averaged spectral absorbance averaged over $\lambda = 1$ μm to $\lambda = 2$ μm is defined as the objective function in the genetic algorithm (GA) optimization, and we can adjust the location of the square air holes to form the complex topology, in order to achieve the highest broadband absorbance. A genetic algorithm (GA) or evolutionary algorithm is a stochastic global search method that mimics the metaphor of natural biological evolution [21]. The principle of survival of the fittest is applied to a population of individuals, which are potential solutions to the problem. Individuals with higher fitness in the problem domain have a better chance to be selected and to reproduce their own offspring. Genetic algorithm has been proved to be effective in many engineering physics subjects [14], [17], [18], [22], [23]. In the case of broadband absorption in MPA, the complexity associated with the topology and the absorption in metal-dielectric stacking undoubtedly leads to a large searching space. Conventional local optimization methods are unlikely to be effective in this case. The optimization of the pattern-designed non-tapered HMM MPAs takes around 100 hours using an Intel™ quad-core Xeon 3.1GHz processor.

3. Numerical Optimization Using Coupled Wave Analysis

Fig. 2 shows the spectral absorbance over $\lambda = 1$ μm to $\lambda = 2$ μm for the pattern-optimized MPA. The top view of the optimized pattern is shown in the inset. The HMM is realized by using aluminum (Al)/ silicon dioxide (SiO_2) stacking. The photonic density of the state is unbounded due to the hyperbolic dispersion. The more realistic picture for the enhanced absorption is that the wave can be confined and propagate in the metal-semiconductor interface. While there are many such surfaces, the absorption is dramatically boosted. In addition to the fact that there are a large number of photonic states in the HMM stack, the coupling of the incoming photon into the HMM is also an important consideration as far as perfect absorption is concerned. This is because the theoretical derivation of the hyperbolic dispersion in HMM assuming an infinite domain of alternating metal-dielectric stacking. In a real application, the alternate metal-dielectric layers can only exist in the semi-infinite domain, and the wave is incident from the domain top boundary. The coupling of the photons into the HMM can be achieved using adiabatic coupling such as in tapered HMM MPA [11], [24]. The effective index is gradually changed from air to the HMM. The pronounced advantage of such a structure is the ultra broadband response. Nevertheless, due to the large index difference

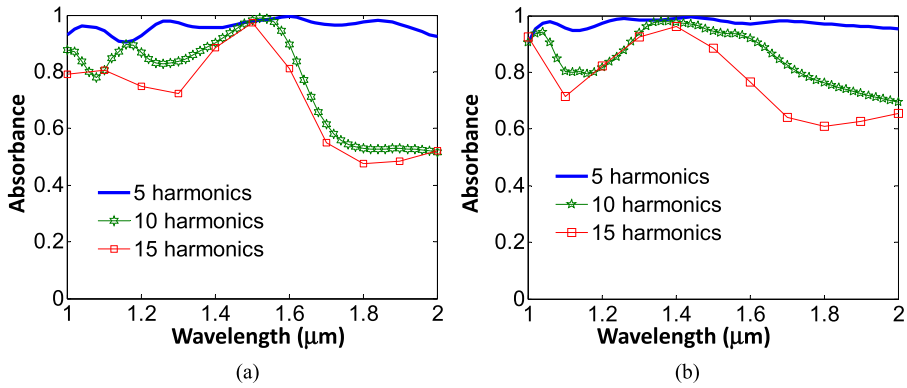

Fig. 3. Spectral absorbance using different RCWA harmonics for (a) TE polarization and (b) TM polarization. The optimization in this work uses 5 harmonics, while more harmonics are possible with a computation parallelization cluster. $t_{Al} = 26.8$ nm, $t_{SiO2} = 18.2$ nm, and $t_{etch} = 360$ nm (eight pairs). The other geometry is listed in the GA 3rd run row of Table 1.

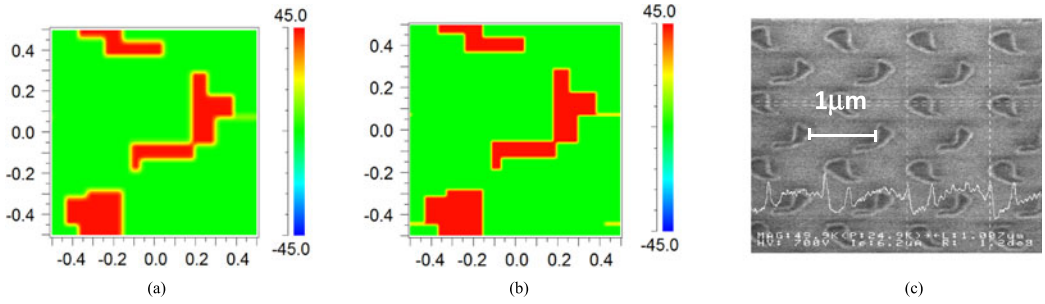

Fig. 4. Comparison between the (a) 5-harmonic synthesized pattern and (b) the 10-harmonic synthesized pattern. (c) Experimentally exposed pattern using Sumitomo™ NEB-22 resist is also shown to compare with the RCWA synthesized pattern by eigenmode expansion. The resolution of NEB-22 is 100 nm. The geometry is the GA 3rd run in Table 1.

between metal and air, a long nano-tip or tapered photonic nanostructures are inevitable, which can lead to process complexity. The structure proposed in this work utilizes the pattern optimization techniques, and it is shown that the photon in-coupling can still be achieved by shape-tailored air cavities.

Due to the high computational demand and the resist resolution limitation, we use the first five harmonics in RCWA, during the GA optimization. Fig. 3 compares the simulation result for 5-harmonic spectral absorption as a result of GA optimization and 10-harmonic simulation result. Additionally, 15-harmonic verification is also provided. A 5-harmonic optimization run already takes $>$100 hours using Xeon 3.1GHz CPU. It is worth to point out that a large number of harmonics in GA may not give better result in experiment. In Fig. 4, we show the patterns synthesized by 5 harmonics and by 10 harmonics in RCWA eigen mode expansion. The details of RCWA, Fourier analysis in optics, and eigenmode expansion can be found in the literature [19], [25], [26]. It can be seen that the 10-harmonic pattern exhibits sharp corners while the 5-harmonic pattern exhibits rounded corners. In the real lithography process using NEB-22 resist, since the resist resolution is $\sim$100 nm, the sharp corners using 10 harmonics will not be resolved. As a result, 5th harmonics is sufficient to form the complex photonic pattern in the HMM structure. The half-wavelength of the 5th harmonic corresponds to 100 nm for our periodic topology-optimized pattern with period $P = 1031$ nm. This means the half-wavelength of the 5th harmonic matches the resist resolution. Higher RCWA harmonics can result in sharp corners in the pattern synthesized by the generalized Fourier series, but such sharp corners cannot be resolved using NEB-22 photoresist. The deviation and error associated with using 5-harmonic RCWA optimization is tolerable, which will be evident

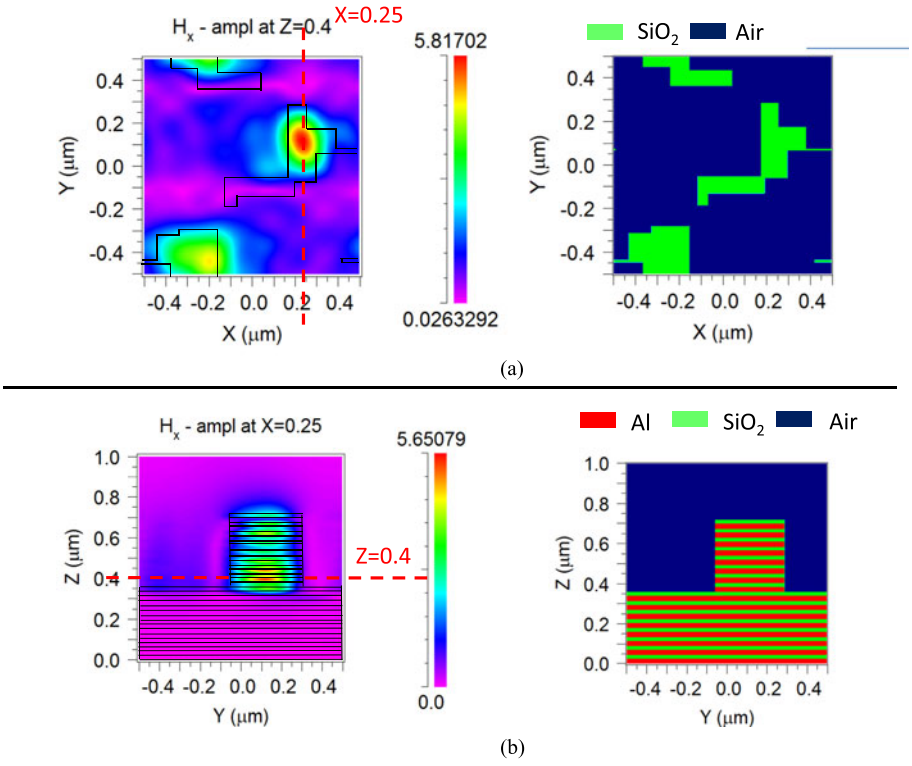

Fig. 5. Field profile, time-harmonic steady state magnetic field amplitude x-component H_x at cross-sections for TE polarization at $\lambda = 1.5$ μm. (a) X-Y cross section at $Z = 0.4$ μm. (b) Z-Y cross section at $X = 0.25$ μm. The index profile is also shown. $t_{Al} = 26.8$ nm, $t_{SiO2} = 18.2$ nm, and $t_{etch} = 360$ nm (eight pairs). The other geometry is listed in the GA 3rd run row of Table 1.

afterward when we examine the experimental result. Certainly, there is still some error using the first five harmonics even if the half-wavelength of the 5th harmonic matches to the resist resolution. As a result, experimental optimization and trial are necessary. We have proposed the Exp-GA procedure previously [27], and the combined optimization of experiment and simulation can be the most computationally manageable and time-efficient. In this work, we do not use complex Exp-GA procedure but only use several trial runs in experiment, and we can locate high broadband absorbance topology.

Fig. 5 shows the field profile at various cross-sections for the 3-D photonic structure. The H_x profile in XY plane at $Z = 0.4$ and YZ plane at $X = 0$ are shown to analyze the origin for the broadband absorption in the metal-dielectric stack with topology optimized patterns. Fig. 5(a) clearly indicates that the field is condensed at the shaped metal-semiconductor region where the absorption in metal is dense. The H_x profile at YZ plane at $X = 0$ in Fig. 5(b) further confirms that the field intensity is condensed at the metal-semiconductor interface. Additionally, from Fig. 5(b), it can be observed that the coupling of the incoming photons is not only in the top-down direction, and the coupling also comes from the side. The incident photons slips into the HMM stack, which is evident from Fig. 5(b) where the lateral propagation of the wave in the y-direction is very evident. We claim the lateral propagation into the structure in Fig. 5(b) because this can be confirmed by seeing that the field intensity is lower at the top of the metal-dielectric stacking and higher in the bottom at $Z = 0.4$ μm, indicating that a significant portion of the optical power is not coupled through the top-down direction. The shaped HMM cavity is beneficial to the wave impedance matching between HMM and air and thus the photon in-coupling, by using diffraction and resonance. Due to the increased photon-incoupling by shape-optimization and the unbounded PDOS associated with the HMM stacking, the pattern-optimized non-tapered MPAs can exhibit broadband absorption.

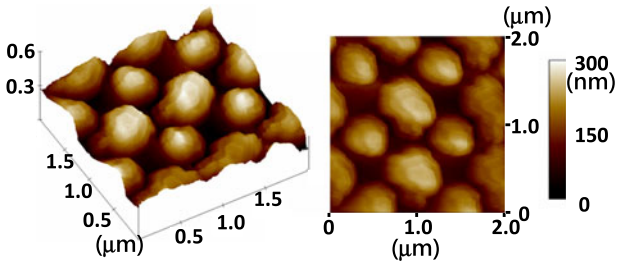

Fig. 6. Atomic force microscope image (AFM) for the pattern-optimized hyperbolic MPA. (Left) 3-D view. (Right) 2-D contour. The geometry is the GA 3rd run in Table 1.

In Section 4, it will be shown that we experimentally achieve an HMM MPA with averaged absorbance 88.38%, which is certainly comparable to other state-of-the-art experimental effort using HMM tapers [9], [10] to date. The elimination of taper can be beneficial if the MPA is to be incorporated with silicon photonic and silicon IC where controlled tapered sidewall or stencil lithography is less compatible.

4. Experimental Result

The preliminary experimental result has been conducted to investigate the broadband characteristics for HMM MPA consisting of SiO_2/Al stacking. The proposed design does not require silver (Ag) and gold (Au) since it does not strongly count on plasmonic effect, and the extinction coefficients of Al is high enough for the topology-optimized MPAs here. Ag and Au are not compatible with silicon cleanroom processing and not suitable for silicon nano-photonics. The fabrication is accomplished using Leica e-beam lithography system using NEB-22 from Sumitomo Chemical™ as the resist. The resolution of the NEB-22 is around 100 nm due to it is a DUV resist, and we use it in conjunction with e-beam lithography here. Thus, the resolution is not limited by the e-beam spot size but by the resist itself. The Lam research® inductive coupled reactive ion etching (RIE) is employed, and we use Cl_2 for Al etching and CHF_3 for SiO_2 etching. The improved pattern accuracy can be attained if a higher resolution resist is employed, which is not very difficult to attain in fact. It should be emphasized that other common lithography techniques such as photolithography and nanoimprint can also be used, and both of these techniques are scalable for large area devices with high throughput. The atomic force microscope (AFM) graphs are shown in Fig. 6, and the spectral absorbance is shown in Fig. 7. The absorbance is significanly boosted by the pattern design where the averaged absorbance is 88.38% over the broadband spectral range $\lambda = 1$ μm to $\lambda = 2$ μm in the best case of Fig. 7(d).

Fig. 7 shows the comparison for samples with various patterns on HMM stack. Fig. 7(a)–(c) is a regular square pattern array etched into the HMM stack. Fig. 7(d)–(f) is pattern-optimized HMM stack in different GA runs. It can be seen that the optimized patterns of different GA runs are somehow different, but the high broadband absorption is all observed with some deviation in performance. Compared with the square-pattern samples, the broadband absorption is significantly boosted by topology optimization, proving the effectiveness of the proposed methodology here. For the square grating comparison, the selection of the filling factor takes come consideration. In the selection of the filling factor, it should be known that the wave impedance of the air and HMM is large, and therefore the etched-away portion should be much greater than the retained portion. As a result, the etched region should be much larger in area compared to the retained, not-etched region. The practice of greater portion of the air-filled region is essential to lower the wave impedance and to reduce the reflection. Consequently, we choose filling factor of 0.85 $\times$ 0.85 in the case of the square air-hole array and 0.5 $\times$ 0.5 and 0.2 $\times$ 0.2 in the square grating. The period is all fixed at 1 μm for the square patterns. It can be seen that in Fig. 7, the pattern optimization is very effective in boosting the spectral broadband absorption. While the current wavelength range is chosen to

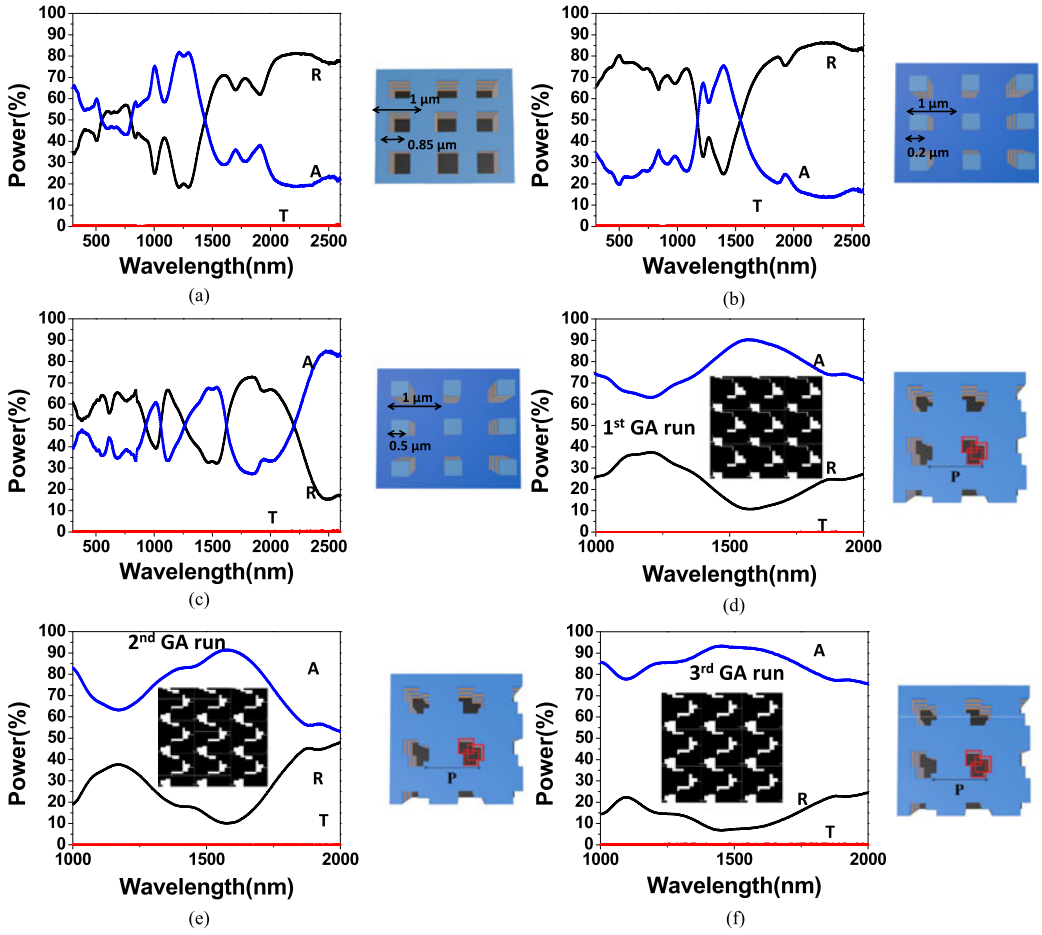

Fig. 7. Spectral absorbance (A), reflectance (R), and transmittance (T) for (a) square air-holes, 0.85 $\times$ 0.85 fill factor, (b) square gratings, 0.2 $\times$ 0.2 fill factor, (c) square gratings, 0.5 $\times$ 0.5 fill factor, (d) the pattern-optimized MPA, the first trial optimization run, (e) the pattern-optimized MPA, the second trial optimization run and (f) the pattern-optimized MPA, the third trial optimization run. The target wavelength range is from $\lambda = 1$ μm to $\lambda = 2$ μm. A quickly mountable type deuterium lamp is used for the ultraviolet region, and a 50W halogen lamp is used for the visible-near-infrared region. The light source is randomly polarized light containing photons of all polarizations.

be $\lambda = 1$ μm $- 2$ μm, the wavelength scalability is actually not very difficult for our design since the aluminum extinction (k) value is large enough for a broad spectral range. This physics behind the pattern optimized HMM MPA is the photon in-coupling by the topology-optimized cavity and the unbounded PDOS of HMM, which do not have strong wavelength dependence. The high extinction (k) of aluminum over a broad spectral range ensures the unbounded hyperbolic dispersion over the broad spectral range. The experimental result is measured using Hitachi U-4100 UV-VS-NIR spectrometer with built-in integration sphere, and all diffraction orders are collected. No polarizer is installed, and thus randomly polarized light is incident on the samples. The accurate measurement result confirms that the 5-harmonic design can be usable while higher order RCWA harmonics are not strongly reflected in our exposed pattern using current NEB-22 resist. Most certainly, the spectral absorption can be pushed toward very close to 100% if a high-resolution resist and high accuracy RCWA can be used. Nevertheless, this can significantly increase the computational load and fabrication cost. The 5-harmoinc optimization already leads to the experimental result of averaged 88.38% wideband absorption, which is comparable to the state-of-art experimental tapered HMM MPA in literature [9], [10].

5. Conclusion

In this work, we proposed a non-tapered HMM perfect absorber. The non-tapered nature is beneficial for large-area applications such as TPV. The underlying physics behind the broadband absorption is the unbounded PDOS associated with the HMM and the pattern optimized air cavity facilitating the photon in-coupling. The topology designed cavity initiates quasi-guided modes that are broadband with reasonably strong confinement. We use a 5-harmonic RCWA simulation to form the complex photonic pattern. The half-wavelength of the 5^{th} harmonic RCWA synthesis field matches the photoresist resolution of 100 nm, and therefore the calculated pattern can be fabricated in lithography. The residual higher-order harmonics are neglected to save the GA optimization runtime, and several experimental trials compensate the potential inaccuracy with 5-harmonic RCWA optimization. The experimentally achieved broadband absorption is 88.38% over $\lambda = 1$ μm to $\lambda = 2$ μm, comparable to the state-of-the-art experimental effort of the tapered HMM MPAs, such as the work by Guo *et al.* [9] and Gan *et al.* [10]. The combined simulation and experiment optimization can be the most time-efficient way toward MPA design with complex topology. The future effort can be employing the fully accurate RCWA and the high-resolution lithography for unity broadband absorption, with the help of computing clusters and 20 nm-resolution lithography.

References

[1] X. Liu, T. Tyler, T. Starr, A. F. Starr, N. M. Jokerst, and W. J. Padilla, "Taming the blackbody with infrared metamaterials as selective thermal emitters," *Phys. Rev. Lett.*, vol. 107, 2011, Art. no. 045901.

[2] C. Wu *et al.*, "Metamaterial-based integrated plasmonic absorber/emitter for solar thermo-photovoltaic systems," *J. Opt.*, vol. 14, 2012, Art. no. 024005.

[3] X. Liu, T. Starr, A. F. Starr, and W. J. Padilla, "Infrared spatial and frequency selective metamaterial with near-unity absorbance," *Phys. Rev. Lett.*, vol. 104, 2010, Art. no. 207403.

[4] K. Aydin, V. E. Ferry, R. M. Briggs, and H. A. Atwater, "Broadband polarization-independent resonant light absorption using ultrathin plasmonic super absorbers," *Nature Commun.*, vol. 2, Art. no. 517, 2011.

[5] J. Hao, J. Wang, X. Liu, W. J. Padilla, L. Zhou, and M. Qiu, "High performance optical absorber based on a plasmonic metamaterial," *Appl. Phys. Lett.*, vol. 96, 2010, Art. no. 251104.

[6] H. Tao, N. I. Landy, C. M. Bingham, X. Zhang, R. D. Averitt, and W. J. Padilla, "A metamaterial absorber for the terahertz regime: Design, fabrication and characterization," *Opt. Exp.*, vol. 16, pp. 7181–7188, 2008.

[7] A. Poddubny, I. Iorsh, P. Belov, and Y. Kivshar, "Hyperbolic metamaterials," *Nature Photon.*, vol. 7, pp. 948–957, 2013.

[8] M. Noginov, M. Lapine, V. Podolskiy, and Y. Kivshar, "Focus issue: Hyperbolic metamaterials," *Opt. Exp.*, vol. 21, pp. 14895–14897, 2013.

[9] J. Zhou, A. F. Kaplan, L. Chen, and L. J. Guo, "Experiment and theory of the broadband absorption by a tapered hyperbolic metamaterial array," *ACS Photon.*, vol. 1, pp. 618–624, 2014.

[10] D. Ji *et al.*, "Broadband absorption engineering of hyperbolic metafilm patterns," *Sci. Rep.*, vol. 4, 2014, Art. no. 4498.

[11] Y. Cui *et al.*, "Ultrabroadband light absorption by a sawtooth anisotropic metamaterial slab," *Nano Lett.*, vol. 12, pp. 1443–1447, 2012.

[12] C. Wang, S. Yu, W. Chen, and C. Sun, "Highly efficient light-trapping structure design inspired by natural evolution," *Sci. Rep.*, vol. 3, 2013, Art. no. 1025.

[13] X. Sheng, S. G. Johnson, J. Michel, and L. C. Kimerling, "Optimization-based design of surface textures for thin-film Si solar cells," *Opt. Exp.*, vol. 19, pp. A841–A850, 2011.

[14] A. Lin and J. D. Phillips, "Optimization of random diffraction gratings in thin-film solar cells using genetic algorithms," *Solar Energy Mater. Solar*, vol. 92, pp. 1689–1696, 2008.

[15] Q.-Y. Wen, H.-W. Zhang, Y.-S. Xie, Q.-H. Yang, and Y.-L. Liu, "Dual band terahertz metamaterial absorber: Design, fabrication, and characterization," *Appl. Phys. Lett.*, vol. 95, 2009, Art. no. 241111.

[16] Y.-C. Lee, C.-F. Huang, J.-Y. Chang, and M.-L. Wu, "Enhanced light trapping based on guided mode resonance effect for thin-film silicon solar cells with two filling-factor gratings," *Opt. Exp.*, vol. 16, pp. 7969–7975, 2008.

[17] S. Preblea, M. Lipson, and H. Lipson, "Two-dimensional photonic crystals designed by evolutionary algorithms," *Appl. Phys. Lett.*, vol. 86, pp. 061111-1–061111-3, 2005.

[18] L. Shen, Z. Ye, and S. He, "Design of two-dimensional photonic crystals with large absolute band gaps using a genetic algorithm," *Phys. Rev. B*, vol. 68, pp. 035109-1–035109-5, 2003.

[19] *Rsoft*, *Rsoft CAD user manual*, 8.2 ed., Rsoft Design Group., New York, NY, USA, 2010.

[20] K. C. Johnson, *Grating Diffraction Calculator (GD-Calc®) –Coupled-Wave Theory for Biperiodic Diffraction Gratings*, 2008.

[21] A. Chipperfield, P. Fleming, H. Pohlheim, and C. Fonseca, Genetic Algorithm Toolbox User Guide, Univ. Sheffield, Sheffield, U.K., 1994.

[22] B. Deken, S. Pekarek, and F. Dogan, "Minimization of field enhancement in multilayer capacitors," *Comput. Mater. Sci.*, vol. 37, pp. 401–409, 2006.

[23] H. Lipson and J. B. Pollack, "Automatic design and manufacture of robotic lifeforms," *Nature*, vol. 406, pp. 974–978, 2000.

[24] C. Argyropoulos, K. Q. Le, N. Mattiucci, G. D'Aguanno, and A. Alu, "Broadband absorbers and selective emitters based on plasmonic Brewster metasurfaces," *Phys. Rev. B.*, vol. 87, 2013, Art. no. 205112.
[25] L. Li, "New formulation of the Fourier modal method for crossed surface-relief gratings," *J. Opt. Soc. Amer. A*, vol. 14, p. 2758–2767, 1997.
[26] M. G. Moharam and T. K. Gaylord, "Rigorous coupled-wave analysis of metallic surface-relief gratings," *J. Opt. Soc. Amer. A*, vol. 3, pp. 1780–1787, 1986.
[27] Y. K. Zhong, S. M. Fu, N. P. Ju, P. Y. Chen, and A. Lin, "Experimentally-implemented genetic algorithm (Exp-GA): Toward fully optimal photovoltaics," *Opt. Exp.*, vol. 23, pp. A1324–A1333, 2015.